HYDRIDING BEHAVIOR OF GAS-ATOMIZED AB_5 ALLOYS

R. C. Bowman, Jr., C. Witham, B. Fultz,
Division of Engineering & Applied Science
California Institute of Technology, Pasadena, CA 9112.5 (USA)

B. V. Ratnakumar
Electrochemical Technologies Group
Jet Propulsion Laboratory
California Institute of Technology
4800 Oak Grove Dr., Pasadena, CA 91109 (USA)

T. W. Ellis, and L E. Anderson
Ames Laboratory
Iows State University
Ames, IA 50011 (USA)

Abstract

"l'he hydriding characteristics of some AB_5 alloys produced by high pressure gas atomization (l-lI'GA) have been examined during reactions with hydrogen gas, and in electrochemical cells. 'l'he hydrogen storage capacities and the equilibrium pressures for I 1 PGA processed 1 $LaNi_5$, $LaNi_{4.75}Sn_{0.25}$, and $MmNi_{3.5}Co_{0.8}Al_{0.4}Mn_{0.3}$ alloys (where Mm denotes Mischmetal) are found to be nearly identical to annealed alloys produced as ingots. The large discontinuous volume change across the α - β plateau region for gas-atomized $LaNi_5H_x$ was seen to produce extensive fracturing in all but the smallest alloy spheres. However, only the largest spheres of the gas-atomized $MmNi_{3.5}Co_{0.8}Al_{0.4}Mn_{0.3}$ and $LaNi_{4.75}Sn_{0.25}H_x$ alloys exhibited any discernible fracturing. The maximum electrochemical storage capacities of the gas-atomized $LaNi_{4.75}Sn_{0.25}$ and $MmNi_{3.5}Co_{0.8}Al_{0.4}Mn_{0.3}$ alloys were found to be smaller than the capacities of annealed alloys prepared from ingots.

Keywords: Metal hydrides, Gas atomization, Electrochemical hydride properties, hydrogen storage alloys, Ni-M H battery alloys, $LaNi_5$

Introduction

Rare earth AB_5 Haucke phase alloys are king used extensively in negative electrodes of rechargeable nickel-metal hydride (Ni-MI 1) batteries. Sakai, et al. [1-3] have described the importance of alloy composition, stoichiometry, and microstructure on both electrode performance and durability during electrochemical charge-discharge cycling. in particular, variations in alloy casting conditions and thermal processing have been shown [1-3] to influence hydrogen absorption-desorption properties and cycle life of mischmetal (Mm) based AB_5 alloys. The recently dcve.loped high-pressure gas atomization (1 HPGA) processing technology [4] may offer benefits associated with rapid- solidification effects, which could enhance Ni-MI 1 battery performance characteristics with lower cost h4n]-base.d alloys. HPGA is being explored as a substitute for the common commercial practice of manufacturing $LaNi_5$ powders from chill-cast ingots that must be extensively annealed to homogenize the cast microstructure prior to mechanical crushing and grinding. An expected advantage for HPGA alloys would be homogencity of the rapidly solidified microstructure [4] that should yield improved hydrogen capacities and less variability in the plateau pressures.

The present study was planned to evaluate the hydriding behavior of some representative AB_5 alloys produced by the HPGA method during gas-phase reactions and during electrochemical cycling in alkaline solutions. These results are compared to measurements performed on similar alloys that were prepared by conventional methods. The specific systems investigated include $LaNi_5$, $MmNi_{3.5}Co_{0.8}Al_{0.4}Mn_{0.3}$ (which corresponds to a particularly robust alloy for electrochemical cycling [2]), and $LaNi_{4.75}Sn_{0.25}$. Substituting tin (Sn) for Ni in $LaNi_5$ has been found to enhance greatly the capacity retention of the material during both thermal cycling with hydrogen gas [5] and in electrochemical cells [6]. The best hydrogen storage capacity and cyclic lifetimes for annealed, arc-melted $LaNi_{5-y}Sn_y$ alloys during electrochemical reactions were found for $y = 0.25$ [6]. This Sn composition should therefore serve as a good test of the properties of materials prepared by HPGA.

Experimental Details

High yields of fine (less than 20 μm diameter) spherical powders of rare-earth AB_5 alloys were produced with the previously described[4] Ames Laboratory HPGA system. Scanning electron micrographs of the particle shapes and size distributions for as-prepared gas-atomized (GA) $LaNi_5$ and $MmNi_{3.5}Co_{0.8}Al_{0.4}Mn_{0.3}$ alloys are shown in Figure 1a and 1c, respectively. X-ray diffraction patterns were obtained using an INEL CPS-120 powder diffractrometer with Co K_α radiation. X-ray diffractometry (XRD) revealed GA-$LaNi_5$ to be single phase with high crystalline quality as indicated by very sharp diffraction peaks while the GA-$MmNi_{3.5}Co_{0.8}Al_{0.4}Mn_{0.3}$ and $LaNi_{4.75}Sn_{0.25}$ alloys gave XRD patterns with broadened peaks and indications of small quantities of secondary phases. Additional characterizations of the microstructure for GA-$LaNi_5$ are reported by Anderson, et al. [4].

The pressure-composition-temperature (pcT) data were obtained with an automated version of a previously described [5] all-metal Sieverts' gas-volumetric apparatus. Surface areas of as-produced and activated, gas-cycled powders were determined by the Brunauer-Emmett-Teller (BET) technique using nitrogen gas in a Micromeritics Model 2360 analyzer.

The electrodes for the cyclic electrochemical lifetime studies contained 76% activated alloy powder, 19% INCO nickel powder as a conductive diluent, and 5% Teflon binder pressed at 570 K onto an expanded nickel screen. NiOOH/$Ni(OH)_2$ served as the counter electrode and a Hg/HgO reference electrode was also used. The electrodes were contained in an o-ring sealed, flooded prismatic glass cell with a 31wt% KOH electrolyte solution. The cell assembly and measurement procedures have been thoroughly described else.whc.rc [6].

Results and Discussion

The room temperature hydrogen absorption and desorption isotherms for GA-$LaNi_5$ activated by an initial absorption-desorption cycle are shown in Fig. 2. The excellent reproducibility between the first and fifth cycles confirms that equilibrium conditions have been established during these runs. Fig. 2 also presents the 300 K isotherm data previously

measured at the University of Vermont by Luo, et al. [7] on a high purity $LaNi_{5.00}$ sample, prepared by arc melting and annealed at 1073 K for a week. No discernable differences in total hydrogen capacity, plateau pressures, hysteresis, or width of the α - β region are noted between the unannealed gas-atomized and annealed arc-melted materials.

Fig. 1b illustrates that extensive fracturing had occurred in the GA-$LaNi_5$ particles with diameters greater than 10- 15 μm. Substantial broadening of the x-ray diffraction peaks, which corresponds to particle size reduction and microstrains induced during hydriding [8], was observed following the isotherm measurements. Furthermore, the BET surface area of the as prepared GA-$LaNi_5$ alloy increased from 0.04 m^2/g to 0.27 m^2/g after the fifth pcT isotherm, which was essentially identical to the 0.21 m^2/g surface area determined on the annealed arc-melted $LaNi_5$ material after the isotherm measurement shown in Fig. 2. Evidently the nominal 25 % unit cell volume expansion across α - β region for the GA-$LaNi_5$ particles produces fracturing and decrepitation when the diameters of the spherical particles exceed about 10 μm.

Due to the widespread commerical interest in Mm-based alloys for Ni-MH batteries, a gas-atomized $MmNi_{3.5}Co_{0.8}Al_{0.4}Mn_{0.3}$ alloy was produced by HPGA. Hydrogen absorption-desorption isotherms were determined at three temperatures after activation. These results are presented in Fig. 3. The plateau pressures for this gas-atomized alloy have significant slopes and hysteresis. Nevertheless, the isotherm for 313 K in Fig. 3 corresponds much more closely to the isotherm reported by Sakai, et al. [2] for induction melted and melt-spun $MmNi_{3.5}Co_{0.8}Al_{0.4}Mn_{0.3}$ alloys than for their gas-atomized powder. Our HPGA method apparently produced a more homogenous composition than the process previously used by Sakai, et al. The SEM micrograph in Fig. 1d shows that only the largest spheres in the activated GA-$MmNi_{3.5}Co_{0.8}Al_{0.4}Mn_{0.3}$ alloy experience any discernible fracturing, perhaps because of the much narrower α - β region for this alloy. No significant increases were noted in the x-ray diffraction peaks following these hydriding reactions.

The storage capacities during room temperature cycling of electrochemical cells fabricated from the GA-$MmNi_{3.5}Co_{0.8}Al_{0.4}Mn_{0.3}$ alloy activated by one. or ten gas-phase absorption-desorption cycles are presented in Fig. 4. The maximum electrochemical storage capacities of these cells with HPGA $MmNi_{3.5}Co_{0.8}Al_{0.4}Mn_{0.3}$ were only about 100 -12.0 mAh/g, which is well below the maximum capacity of 250 mAh/g shown in Fig. 4 for an induction melted alloy of similar composition obtained under identical conditions. It is possible that the poor electrochemical behavior of the gas-atomized AB_5 alloy results from the lack of fracturing of stable and tenacious surface corrosion films since the activation procedures generated very little fracturing as shown in Fig. 1d.

Hydrogen absorption and desorption isotherms were measured at room temperature (i.e., 296 K) for unannealed GA-LaNi4.75Sn0.25 after five activation cycles. These results are compared in Fig. 5 to the room temperature (i. e., 3(X) K) isotherms obtained by Luo, et al. [9] on annealed arc-melted $LaNi_{5-y}Sn_y$ with y = 0.1, 0.25, and 0.32. Although the hydrogen storage capacities for both y = 0.25 alloys are nearly identical, the isotherms for the HPGA material exhibit rather steep slopes across the plateau region and a larger hysteresis ratio. Luo, et al. [9] found very similar differences between unannealed and annealed (1073 K for 3d) arc-melted $LaNi_{4.77}Sn_{0.23}$, which is commonly attributed [5, 9,10] to an inhomogeneous distribution of Sn within the microstructure. This interpretation is consistent with the plateau pressures given in Fig. 5 for Sn compositions between y = 0.1 and y = 0.32. It is also consistent with the broadened x-ray diffraction peaks for the GA-LaNi4.75Sn0.25 compared to either GA-$LaNi_5$ or annealed $LaNi_{5-y}Sn_y$. Although the sloping plateau for GA-$LaNi_{4.75}Sn_{0.25}$ is nearly as wide as for GA-$LaNi_5$, SEM micrographs after five activation cycles revealed no fracturing for particles up to 40 μm in diameter. In addition, the surface area only increased from an initial value of 0.06 m^2/g for the as-prepared powder to 0.09 m^2/g following the activation cycles. As seen in the GA-mischmetal alloy, activation did not change the x-ray diffraction peaks of the GA-LaNi4.75Sn0.25 alloy. Hence an inhomogeneous

distribution of Sn appears to prevent microcracking upon hydrogenation at least as well as a homogeneous distribution.

The electrochemical cycling behavior for two cells prepared with unannealed GA-$LaNi_{4.75}Sn_{0.25}$ are compared in Fig. 6 to the capacity for an electrode produced with annealed arc-melted $LaNi_{4.75}Sn_{0.25}$. The HPGA alloy required nearly 20 cycles to give a maximum capacity of 225 - 250 mA/g while the annealed, arc-melted alloy achieved 315 mA/g within five electrochemical cycles. The reduced capacity for the HPGA alloy can be readily attributed to its sloping isotherms where one atmosphere pressure is reached at a hydrogen composition of $x = 5.0$ while one atmosphere is not reached until $x = 5.7$ for the annealed alloy (Fig. 5). An electrochemical capacity at least 15% smaller is therefore predicted for the HPGA alloy. Furthermore, the capacity retention of the HPGA alloy during electrochemical cycling is seen to be less than for the arc-melted alloy (Fig. 6), which when combined with the slower activation also contributes to a reduced maximum capacity. Further discussion of the electrochemical degradation of the HPGA alloys will be presented elsewhere.

In conclusion, GA-AB_5 powders produced by the HPGA method have gas-phase hydrogen storage capacities and equilibrium pressures similar to materials prepared from annealed ingots [2, 5, 7-9]. When used in electrochemical cells, however, unannealed HPGA $MmNi_{3.5}Co_{0.8}Al_{0.4}Mn_{0.3}$ and $LaNi_{4.75}Sn_{0.25}$ have reduced capacities and more rapid degradation than conventionally processed alloys. It is anticipated that substantial improvement in these electrochemical properties can be obtained by appropriate annealings [3] of the gas-atomized alloys. These studies are in progress.

Acknowledgments

This work was carried out at the California institute of Technology and at the Jet Propulsion Laboratory through **an** agreement with the National Aeronautics and Space Administration and was sponsored by the U.S. Department of Energy, Grant DE-FG03-94ER14493. The authors thank Fran **Laabs** (Ames Lab) for the SEM measurements and Prof. Ted Flanagan (U. Vermont) for providing his isotherm data on the annealed $LaNi_{5-y}Sn_y$ alloys. The gas-atomization work was carried out at the Ames Laboratory, 1 owa State University under the U. S. Department of Energy Contract No, W-7405-Eng-82.

References

[1] T. Sakai, H. Yoshinaga, H. Miyamura, N. Kuriyama, and }1. 1 shikawa, J. Alloys Compounds **180** (1992) 37.

[2] T. Sakai, H. Miyamura, N. Kuriyama, H.Ishikawa, and 1. Uehara, Z. Physk. Chem. 183 (1994) 333.

[3] T. Sakai, M. Matsuoka, and C. Iwakura, in Handbook on the Physics and Chemistry of Rare Earths, Vol. 21, Eds.K. A. Gschneider and L. Eyring (Elsevier, Amsterdam 1995), p. 133.

[4] I. E. Anderson, M. G. Osborne, and T. W. Ellis, JOM 48, No. 3 (1996) 38.

[5] R. C. Bowman, Jr., C. H. Luo, C. C. Ahn, C. K. Witham, and B. Fultz, J. Alloys Compounds 217 (1995) 185.

[6] B. V. Ratnakumar, C. Witham, R. C. Bowman, Jr., A. Hightower, and B. Fultz, J. Electrochem. Sot. (In Press).

[7] W. Luo, S. Luo, J. Clewley, T. Flanagan, R. Bowman, J. Cantrell, J. Alloys Compounds 202 (1993) 147.

[8] A. Percheron-Guegan, C. Lartique, J. C. Achard, P. Germi, and F. Tasset, J. Less-Common Met. 74(1980) 1.

[9] S. Luo, W. Luo, J. D. Clewley, T. B. Flanagan, and L. A. Wade, J. Alloys Compounds **231** (1995) 467.

[10] S. Luo, W. Luo, J. D. Clewley, 'l'. B. Flanagan, and R. C. Bowman, Jr., J. Alloys Compounds **231** (1995) 473.

Figure Captions

Fig. 1. Scanning electron microscopy micrographs of gas-atomized alloys: (a) as-prepared $LaNi_5$; (b) GA-$LaNi_5$ after activation and five hydrogen absorption-desorption cycles; (c) as-prepared $MmNi_{3.5}Co_{0.8}Al_{0.4}Mn_{0.3}$ alloy; and (d) GA-$MmNi_{3.5}Co_{0.8}Al_{0.4}Mn_{0.3}$ after ten hydrogen absorption-desorption cycles following activation.

Fig. 2. Comparison of hydrogen absorption (open symbols) and desorption (closed symbols) room temperature isotherms for 1223 K annealed arc-melted and unannealed gas-atomized $LaNi_5$.

Fig. 3. Hydrogen absorption-desorption isotherms for an unannealed gas-atomized $MmNi_{3.5}Co_{0.8}Al_{0.4}Mn_{0.3}$ alloy.

Fig. 4. Comparison of electrochemical storage capacities for activated (1 cycle and 10 cycles) gas-atomized $MmNi_{3.5}Co_{0.8}Al_{0.4}Mn_{0.3}$ and an activated commercial $Mm(NiCoAlMn)_5$ alloy prepared by induction melting.

Fig. 5. Comparison of hydrogen absorption (open symbols) and desorption (closed symbols) room temperature isotherms for unannealed gas-atomized $LaNi_{4.75}Sn_{0.25}$ alloy and for annealed arc-melted $LaNi_{5-y}Sn_y$ with $y = 0.1$, 0.25, and 0.32 determined by Luo, et al. [9].

Fig. 6. Comparison of electrochemical storage capacities for the activated gas-atomized and annealed arc-melted $LaNi_{4.75}Sn_{0.25}$ alloys.

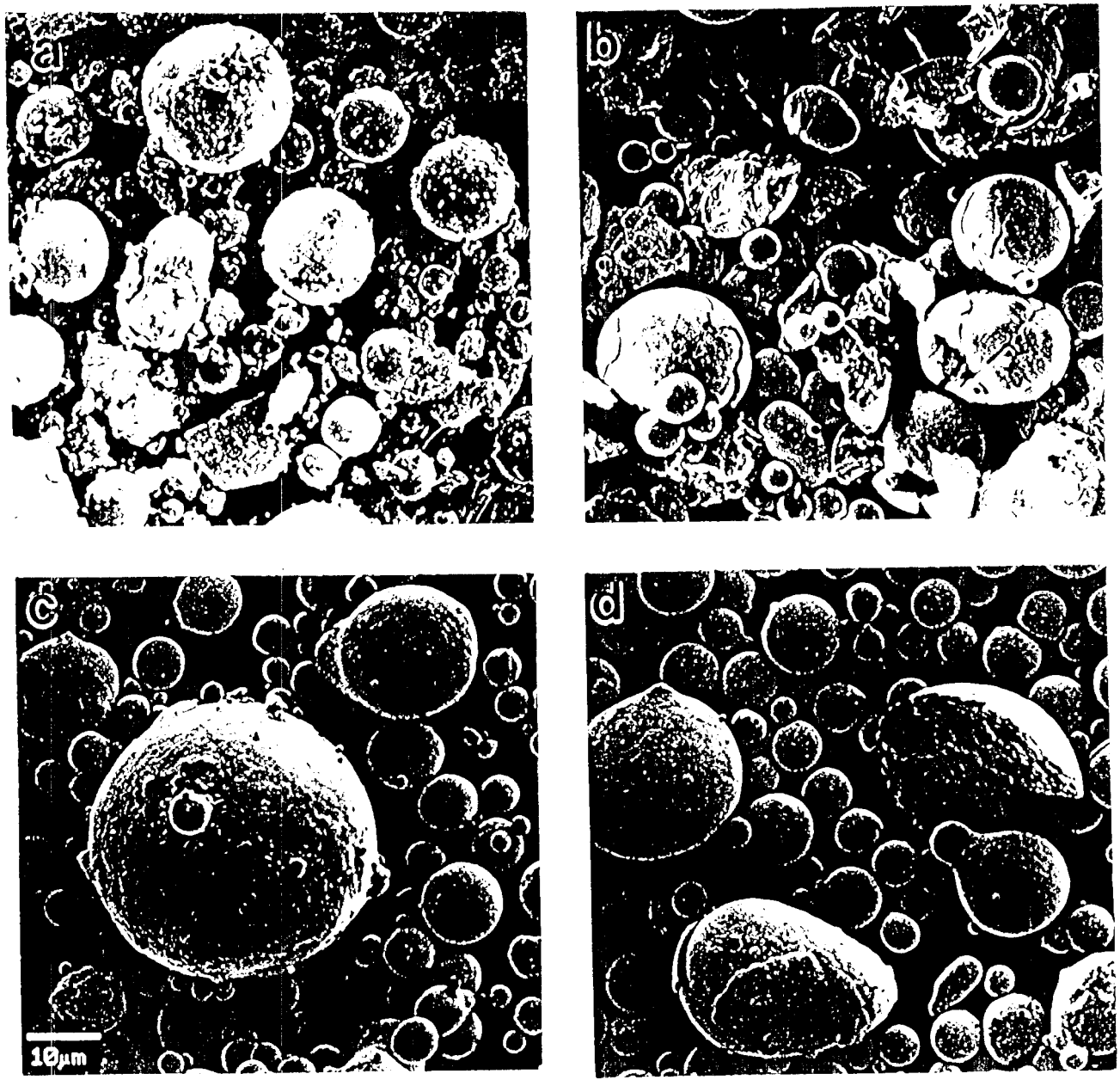

Figure 1

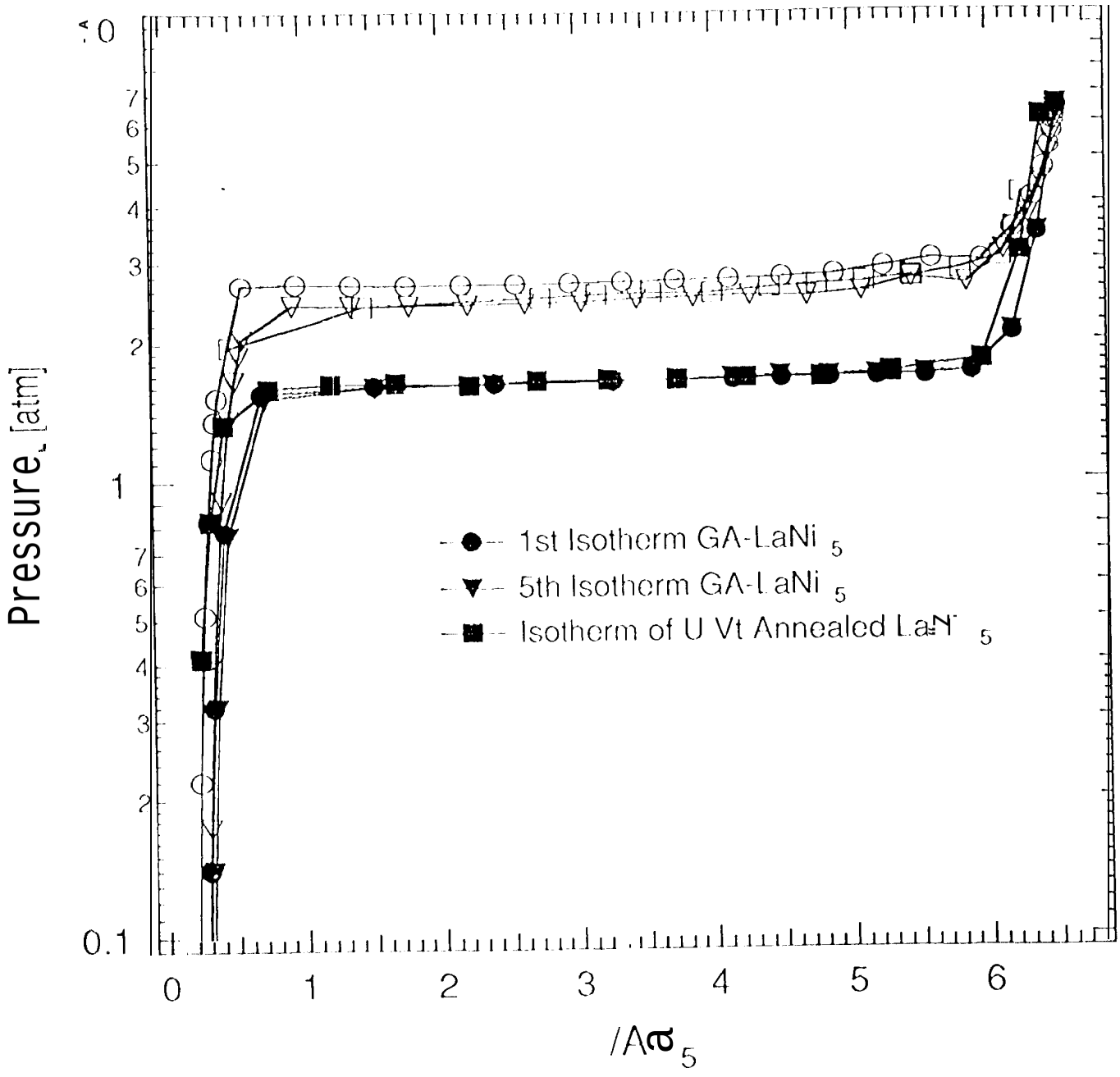

Bowman, et al

igure 2

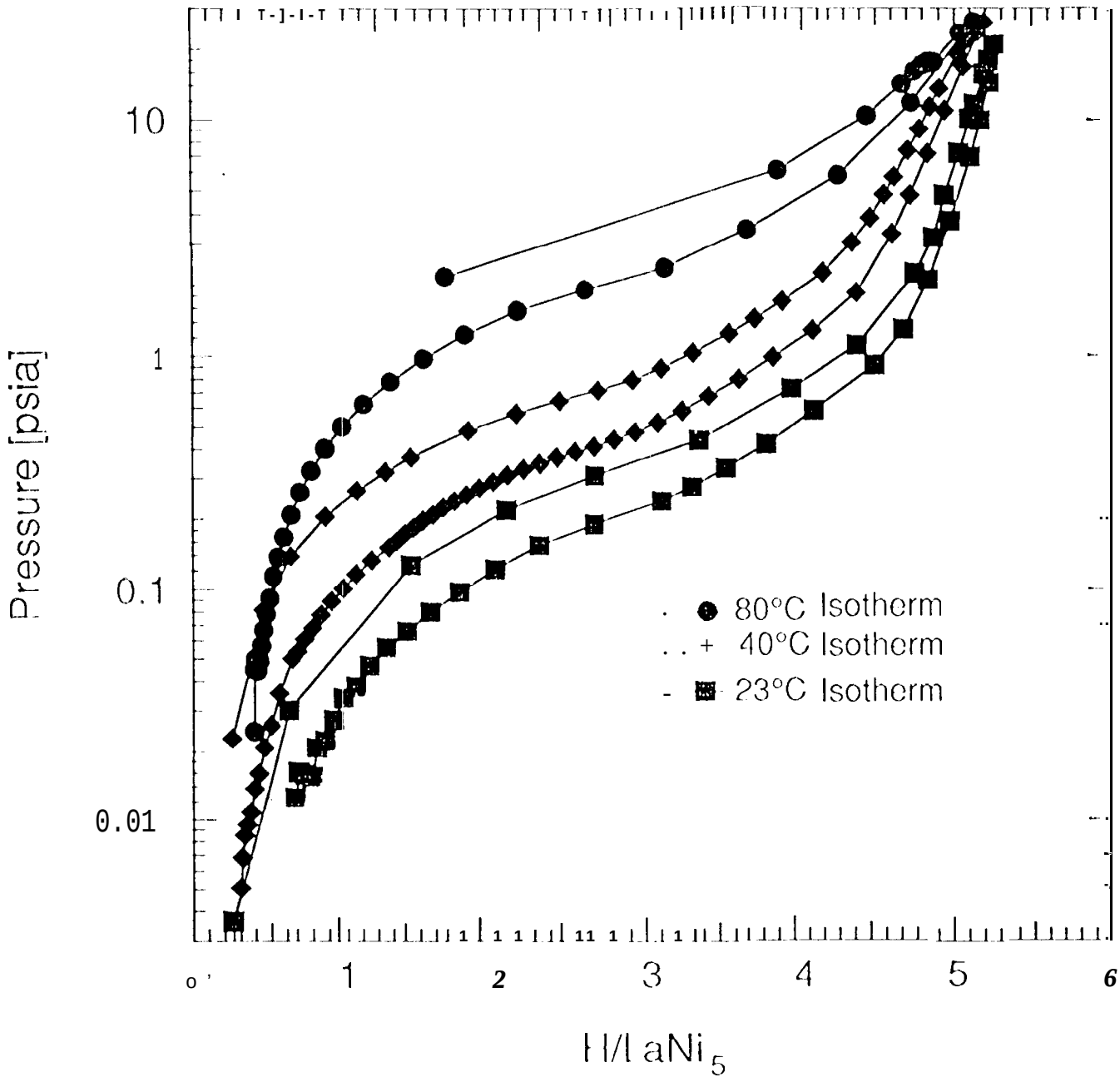

Bowman, et. al

Figure 3

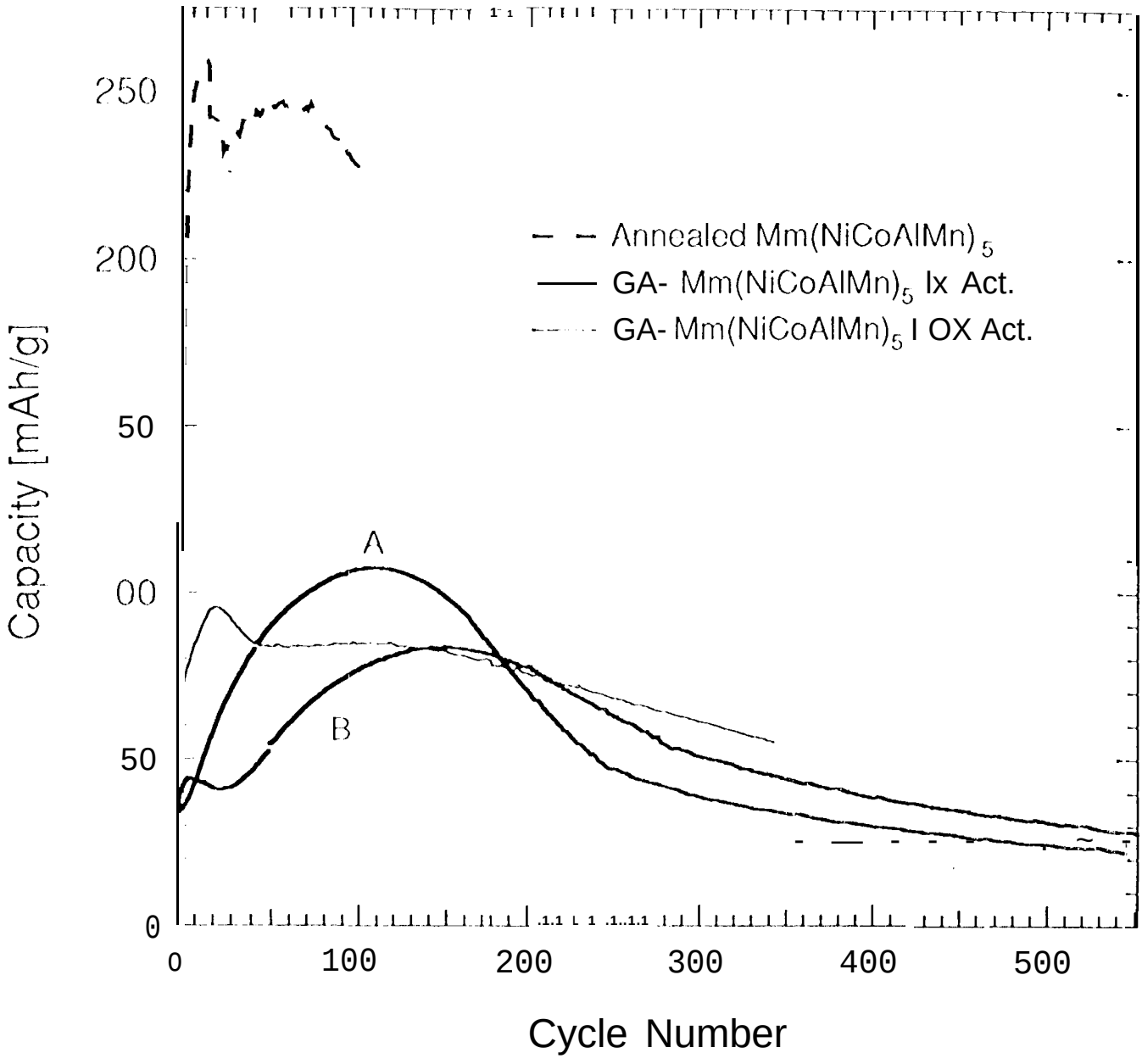

Bowm an, et al

figure 4

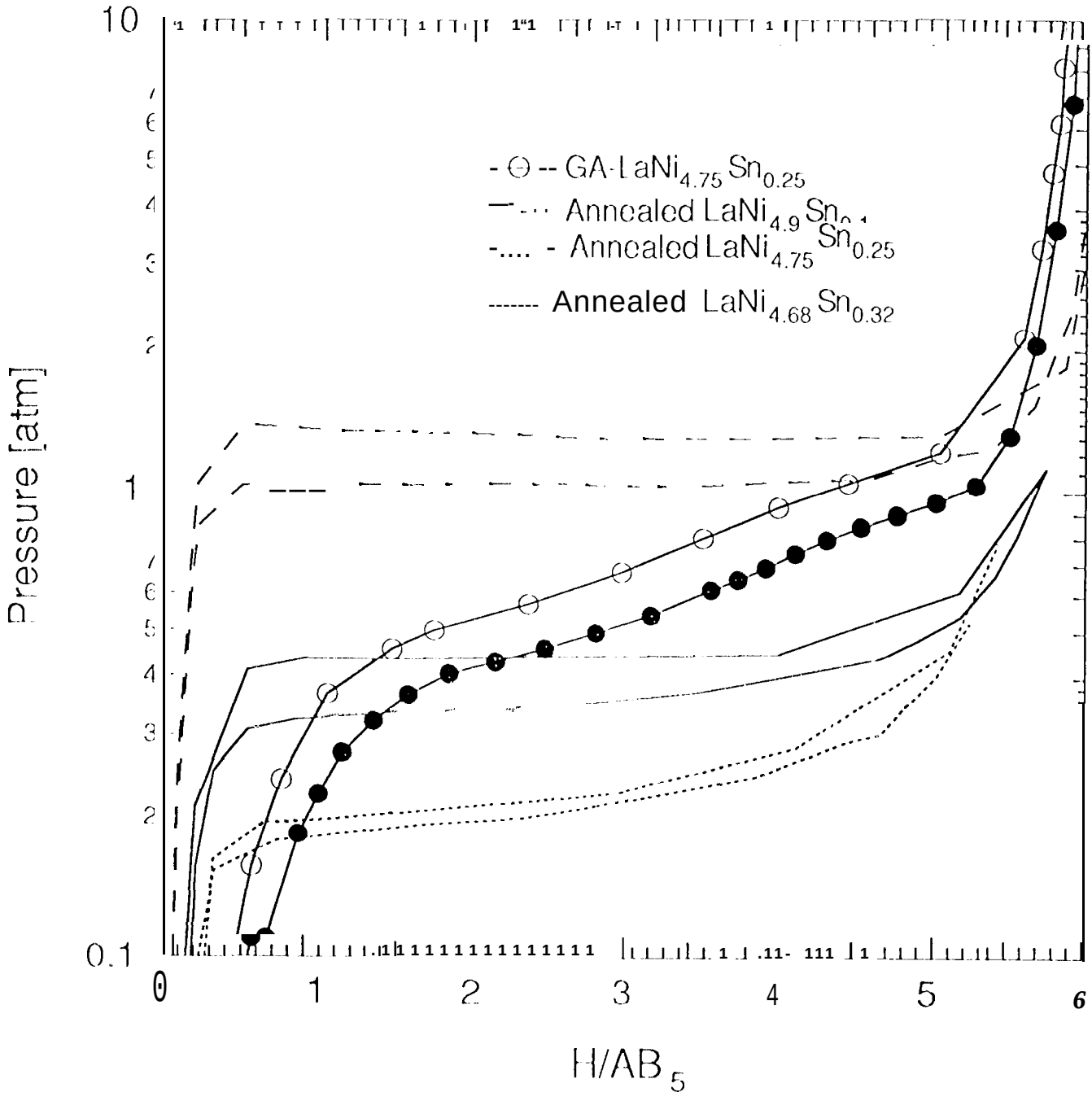

Bowman, et. al

Figure 5

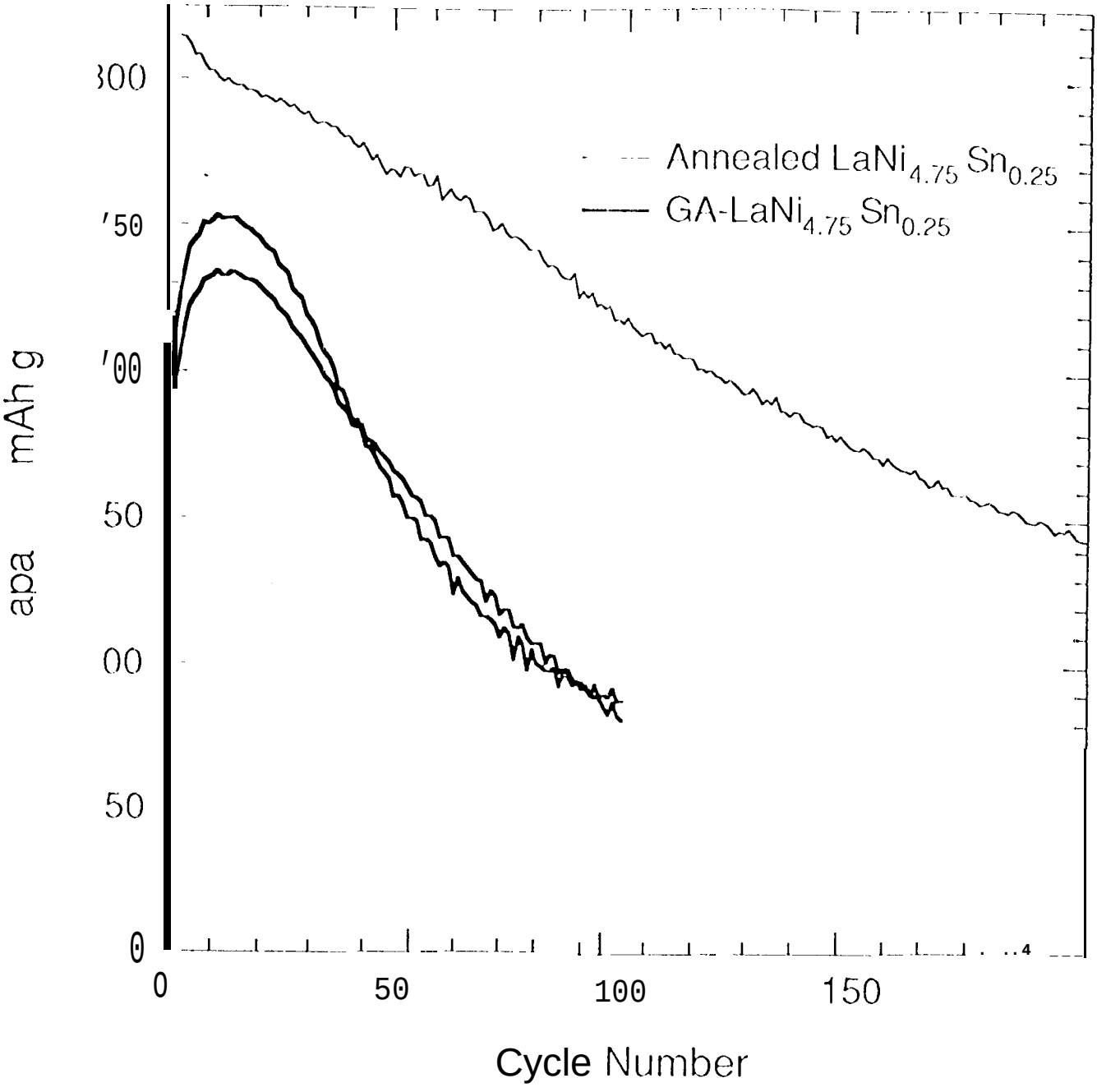

Bowman, et. al

Figure 6